ACS NANO

www.acsnano.org

ARTICLE

Tough and Strong: Cross-Lamella Design Imparts Multifunctionality to Biomimetic Nacre

Hemant Kumar Raut, Alan F. Schwartzman, Rupambika Das, Fan Liu, Lifeng Wang, Caroline A. Ross,* and Javier G. Fernandez*

Cite This: https://dx.doi.org/10.1021/acsnano.0c01511

Read Online

ACCESS | Metrics & More | Article Recommendations | Supporting Information

ABSTRACT: The creation of structural composites with combined strength, toughness, low density, and biocompatibility remains a long-standing challenge. On the other hand, bivalve marine shells—*Clinocardium spp.*—exhibit strength, stiffness, and toughness that surpass even that of the nacre that is the most widely mimicked model for structural composites. The superior mechanical properties of *Clinocardium spp.* shells originate from their cross-lamella design, comprising $CaCO_3$ mineral platelets arranged in an "interlocked" herringbone fashion. Reproduction of such hierarchical designs could offer multifunctionality, potentially combining strength and toughness at low densities, and the capability for seamless integration with biological systems. Here, we demonstrate manufacturing of the cross-lamella design by biomineralizing aragonite films with sawtooth patterns and assembling them in a chitosan/fibroin matrix to generate a composite with interlocked mineral layers. The resultant composite, with a similar constitution to that of the biological counterpart, nearly doubles the strength of previous nacre-mimetic composites while improving the tensile toughness and simultaneously exhibiting stiffness and biocompatibility.

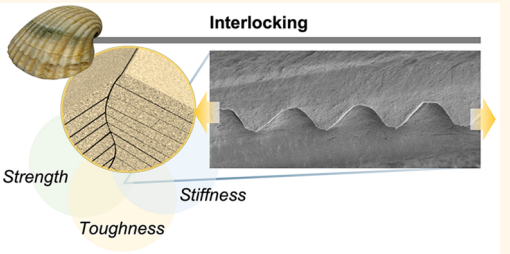

KEYWORDS: *bioinspired composite, cross-lamella design, nacre, biomineralization, manufacturing, chitosan*

Bioinspired manufacturing—in the sense of replicating the way nature fabricates—holds great potential for supporting technological transformations in a variety of fields, from general manufacturing to medicine.[1] Bioinspired materials are produced by linking the structural components of life with the hierarchical designs with which they have evolved.[2] By doing so, biological molecules not only become relevant for engineering applications due to their abundance and/or integration with biological systems (*e.g.*, human host or ecological cycle) but also become necessary for reproducing the synergies behind the extraordinary mechanical properties of structural biomaterials.

One key property of structural biocomposites is their multifunctionality, which enables a single material to perform satisfactorily in the many multidimensional loading scenarios that an organism may face during its life.[3] Mollusk shells, fish scales, arthropod exoskeletons, mammalian bones, and sponge spicules are examples of such natural composites that exhibit such a remarkably rich and isotropic combination of mechanical properties.[4,5] All these materials, despite their evolutionary disconnection and different compositions, are made of hard but brittle inorganic minerals and soft organic phases. However, the strength and toughness of these composites are orders of magnitude higher than those of their constituents,[6] and they result from the arrangement of the hard and soft phases in the composite matrix.[7] In the paradigmatic example of nacre seashells, the hard-mineral platelets are sandwiched between soft, submicron layers of organic macromolecules, which is one of the most followed models for the synthesis of high mechanical performance artificial materials.[7]

Current approaches to producing biomimetic nacre using its native components focus on the reproduction of a "planar lamellar" model, where the mineral platelets organize parallel to each other across different levels.[8,9] Even this simplified model of nacre, which can be reproduced by freeze-casting,[10,11] slip/tape casting,[12] layer-by-layer bonding,[13,14] and vacuum-assisted filtration,[15] has demonstrated outstanding results in

Received: February 20, 2020
Accepted: June 29, 2020
Published: June 29, 2020

the reproduction of nacre's toughness. However, the strength of nacre-mimetic composites along the platelets remains lower than that of the biological counterpart.[16] Although introduction of nanoscale bridges between inorganic platelets,[17−19] laterally interlocked platelets,[20] and 3D printed platelet geometries[21,22] has yielded improvements in mechanical properties in these composites, the microlevel design of mineral platelets has not been fully considered yet. In particular, planar lamellar models assume that the mineral platelets of nacre arrange in a brick wall structure where the mineral "bricks" have flat interfaces. By contrast, in native nacre, mineral platelets have a wavy cross-section, which causes transverse interlocking between adjacent platelets to increase the composite's resistance to deformation and prevent localized strain.[23,24] An extreme case of this mineral-interlocking can be observed in the inner crossed-lamellar design of the shells of some mollusks, where mineral interlocking occurs at the first-order domain;[25] instead of the mineral plates being "stacked" in a parallel manner, they are slanted toward the adjacent domain, resulting in intricate herringbone patterns (Figure 1a). This interlocking strategy in structural materials is shown across different species in different forms. For instance, the shells of cockles (*Clinocardium spp.*) have periodic inner crossed-lamellar structures,[26] while the conch shell (*Strombus gigas*) has a pattern where the orientation of the crossed-lamellar design changes (from 45° to 90°) in different regions of the shell, resulting in one of the toughest known materials.[27] Notably, this interlocking strategy in structural biocomposites goes beyond mollusks; it is found in other phyla, such as the mineralized microridges in the exoskeleton of sea urchins (*Phormosoma placenta*),[28,29] and even in other kingdoms, such as the teeth-like interlocked mineral shells of diatoms,[30] which is a perfect example of convergent evolution.

RESULTS AND DISCUSSION

Here, we report combined strength, stiffness, and toughness in a biomimetic composite by reproducing the internal structure and composition of the shells of cockles by a distinctive approach of biomineralizing microscopically patterned aragonite platelets and assembling them hierarchically into an "interlocked" architecture across the composite. In the shells of cockles, the mineral platelets (constituting the first-order lamella) are stacked against the next domain at an angle of 30−40° (Figure 1a,b). We replicated the localized biomineralization in natural systems using poly(acrylic acid) (PAA)-induced aragonite biomineralization and microstructured chitosan films (Figure S1).[31−33] This resulted in larger mineral platelets as the PAA−Ca^{2+} complex being adsorbed and subsequently covering the entire chitosan surface (Figure 1c). With the increasing packing density, the adsorbed layer eventually underwent an amorphous-to-crystalline transition, leading to the formation of aragonite, as confirmed by X-ray diffraction (Figure S2a). Areas of several square centimeters (3 × 1 cm^2) of chitosan films with micrometric topography were mineralized by this approach (Figure 1c and Figure S3). Notably, the only factor that limited the size of the patterned aragonite was the size of the reusable mold used for patterning the chitosan films used as a template; by using polymer casting, chitosan films with nanometric features have been produced over large areas,[34] which is the same low-cost, high-throughput technology that is used here, highlighting the readiness of this approach to scale up to an industrially relevant level.

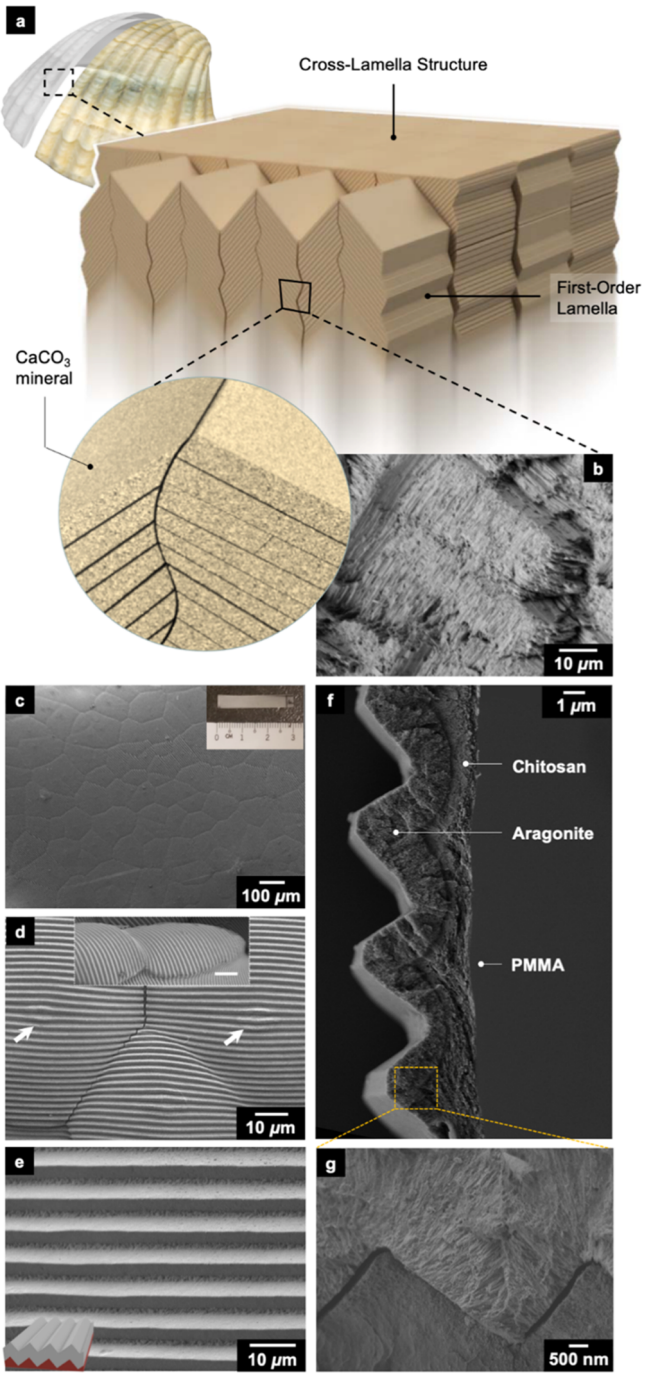

Figure 1. Cross-lamella structures of the shell of *Clinocardium sp.* and its first-order lamella replicated by biomineralization. (a) Schematic of the shell's cross-lamella structure comprising hierarchical first-order lamella. (b) SEM image of the first-order lamella showing the mineral platelets stacked in a herringbone fashion. (c) Biomimetic synthesis of the first-order lamella in the form of patterned aragonite ($CaCO_3$) platelets on patterned chitosan film. The patterned aragonite platelets cover several square centimeters of the chitosan film (photograph shown in inset). (d) The patterned minerals show *Voronoi*-like packing (indicated by the arrows) typically seen in poly(acrylic acid)-induced biomineralization of $CaCO_3$. (e) Magnified view of the first-order lamella comprising a regular ∼5 μm sawtooth profile. (f) Cross-sectional image of the first-order lamella showing the chitosan−aragonite interface. (g) Magnified view of the aragonite mineral showing hierarchical column-like mineral substructures.

https://dx.doi.org/10.1021/acsnano.0c01511
ACS Nano XXXX, XXX, XXX−XXX

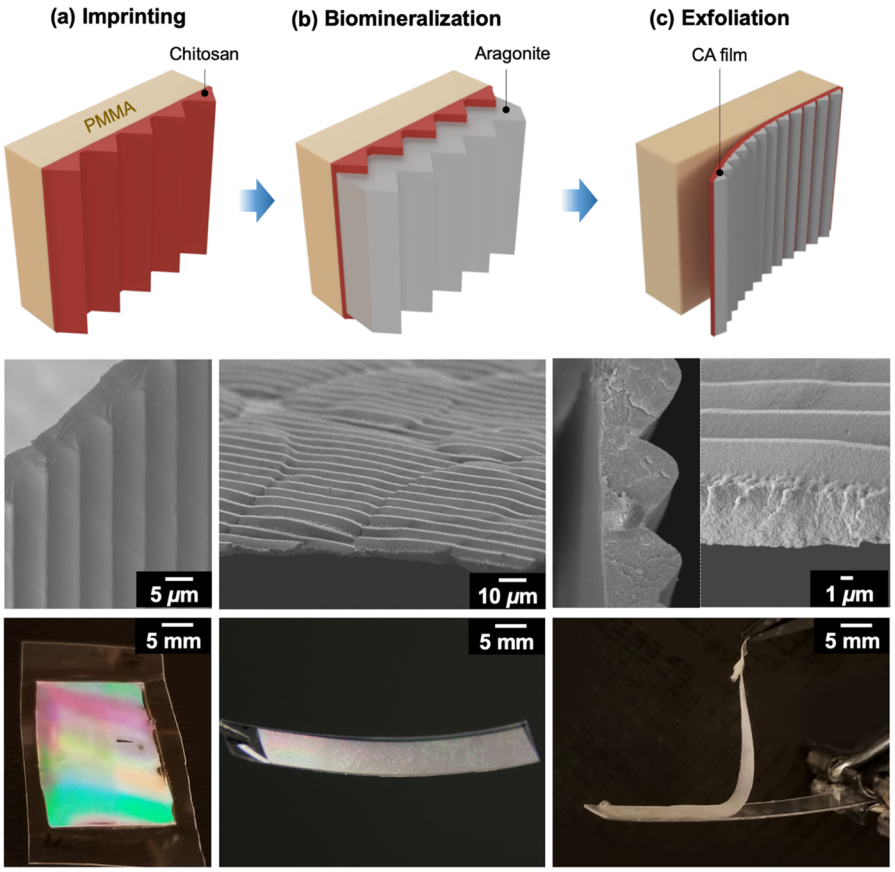

Figure 2. Exfoliation of the patterned mineral layers. (a) Patterned chitosan films were imprinted on flexible PMMA sheets by using a PDMS mold. The patterned chitosan film has a sawtooth cross-section, as shown in the SEM image (middle), and can be imprinted with minimal defects (bottom). (b) The patterned chitosan films are then immersed in the PAA-based $CaCO_3$ precursor to perform biomineralization. This results in the formation of the patterned aragonite minerals on the patterned chitosan film (SEM image shown in the middle). A photograph of the as-mineralized chitosan−aragonite (CA) films is shown in the bottom. (c) After mineralization, the CA films are exfoliated from the PMMA sheet. The front- and side-view SEM images of the free-standing CA films (shown in the middle) gradually peeled-off from the PMMA backing sheet without any damage to the former are shown at the bottom.

Layer by layer, using chitosan films with grating-like patterns, we built the crossed-lamellar structure analogous to the shells of cockles (Figure 1d). While we focused on the reproduction of the inner structures of the shell model, the ability to control the geometry of the aragonite platelets using patterned chitosan was observed to be quite general. Without aiming to explore the global limits of the approach but rather those relevant for this study, we found no apparent constraints to producing mineralized platelets with features ranging from 5 to 2 μm and multiple geometries (Figure 1d,e and Figure S2b,c). In the specific case of the sawtooth-like patterned features, the aragonite conforming to the chitosan patterned films was grown to a thickness of ~5 μm (Figure 1f). Interestingly, a more detailed study of the mineral platelets revealed that the patterned aragonite layers had a hierarchical substructure, resembling the meso-crystal morphology of the mineral component of natural nacre[23,24] (Figure 1g). Formation of such hierarchical mineralized structures has been attributed to the nonclassical pathways of crystallization that involve an amorphous-to-crystalline transformation, such as that used here.[35]

The main challenge to fabricating a hierarchical composite using freestanding films of a few microns thickness is the process of handling and stacking each layer individually. For this purpose, we developed a strategy to exfoliate the patterned chitosan−aragonite (CA) films from the backing of a supporting poly(methyl methacrylate) (PMMA) substrate. By optimizing the thickness of the PMMA and CA films, the latter spontaneously delaminated from the support due to differential shrinking during dehydration (Figure S4). This approach enabled the production of structured films of chitosan on PMMA substrates (Figure 2a), growth of the aragonite platelets (Figure 2b), and separation of the resulting ~7 μm thick freestanding CA fragile layers without inducing any mechanical stress on them (Figure 2c).

The CA films were successively stacked with a fixed volume of silk fibroin solution, which was dispensed between each layer (Figure 3a), an approach that we have successfully used in the past to produce chitosan−fibroin laminates (*i.e.*, Shrilk).[36] In total, nearly 300 CA films were stacked (Figure 3b) with fibroin bonding the films together (Figure S5). Importantly, the fabrication approach enabled the patterned side of adjacent CA films to face each other, thereby forming a laterally "interlocked" arrangement (Figure 3c) of CA films. Finally, the composite was pressed together to avoid air entrapment and flatten the layers (Figure S6), and dried in ambient conditions, which consolidated it to a ~1.5 mm thick composite with a 70.4 ± 1.8% mineral content (Figure S7). Objects that are manufactured with chitinous polymers tend to shrink after manufacturing, which causes warping distortion

https://dx.doi.org/10.1021/acsnano.0c01511
ACS Nano XXXX, XXX, XXX−XXX

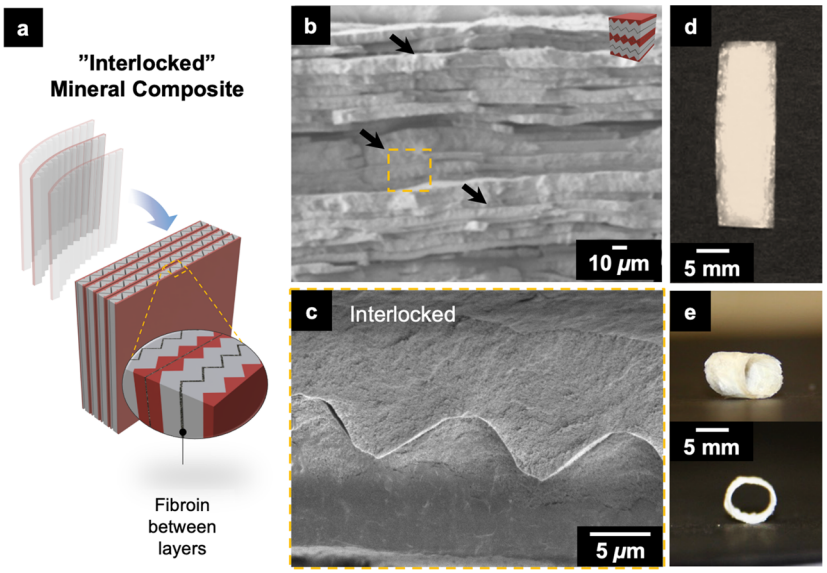

Figure 3. Fabrication of the interlocked mineral composite. (a) Schematic showing the fabrication of the composite by stacking the patterned CA films and infiltrating with silk fibroin (SF) solution. (b) Cross-section of the composite comprising ~300 CA films. The arrows indicate areas where the patterned cross-sections are visible. (c) Magnified view of the composite revealing "interlocking" between the layers. This is achieved by making the patterned side of the CA films face each other during the fabrication. (d) The layer-by-layer bonding approach enables fabrication of mineralized composites with negligible structural shrinkage and unrestricted geometries and sizes. (e) Fabrication of the composite on cylindrical molds enables formation of tubular-shaped nacreous composites.

and variation from the intended geometry (Figure S8) and thus limits their capability to be cast using standard molds.[36] The inclusion of the mineral phase in the matrix reported here resulted in a sturdy composite that conformed to the intended geometry after drying (Figure 3d). As we demonstrated in the past,[37] freestanding chitosan films can be dried on a macroscopic mold to retain their geometry. As expected, the mineralized composites show a higher stiffness (E_r = 20.4 ± 5.4 GPa) than that of the nonmineralized counterpart (evident from the slope of the unloading part of the indentation curves of both composites in Figure 4a). The stiffness of the mineralized composite is albeit lower than natural nacre due to the relatively lower mineral content of ~70% vol. than that of nacre's ~95% vol. Nevertheless, the layer-by-layer bonding approach presented here enabled fabrication of nacreous composites diverging from typical flat shapes. Tubular shapes (Figure 3e) were produced by drying the mineralized layers on cylindrical molds. We believe this demonstration of manufacturing of a nonplanar biomimetic nacre would help the general use of these composites in engineering applications.

The interlocked mineral composite was observed to have simultaneously high ultimate tensile strength (~48 MPa) and nearly 4 times higher tensile toughness (area under the tensile stress−strain) in comparison to that of the planar mineral composite, while matching the stiffness (~25.8 GPa) and density (~(1.51 ± 0.74) × 10^3 kg/m^3) of previous biomimetic nacres (Figure 4a and b).[10] A summary of all the mechanical properties of the interlocked mineral and planar mineral composites is provided in Supporting Information, Table S1. The tensile strength of the interlocked mineral composite (43.59 ± 4.5 MPa) is ~85% higher than that of the planar mineral composites that were produced using the same methodology (23 ± 2.8 MPa) (Figure 4b) and is also close to that of the nacre species *Anodonta woodiana* reported in the literature.[18] The reason for the improvement in tensile strength of the interlocked mineral composite can be understood from finite element analysis of the composites (Figure 4c−e). In the interlocked-mineral composites, the mineral interlocking enables stress transfer through the stiffer mineral phase as opposed to stress transfer through the softer matrix in the case of the planar mineral composite. This helps increase the tensile strength of the interlocked mineral composites in comparison to that of the planar counterpart.[38] This is evident from Figure 4e, showing the maximum principal stress field of composites under same tensile load, that shows that more load can be transferred directly through the interlocked stiffer mineral phase than that of the planar mineral composite. In fact, in previous works on nacre-mimetic composites, the load transfer through the soft organic layer between planar platelets is implicated for the eventual failure of the composite (platelet pull-out is observed when platelets' aspect ratio is less than a critical value). Hence, ways to arrest the sliding of the platelets (*e.g.*, by incorporating nanoscale bridges between platelets) is emerging as a proven strategy to improve their tensile strength.[18,21] Interestingly, our interlocked mineral composite nearly doubled the strength that was reported for the best nacre replicas to date (Figure 5),[10] which follow a planar lamella model and are produced using an "assembly-and-mineralization" approach. Additionally, the similar mechanical strength of our planar mineral composite presented here and those produced previously (Figure 5), when considered independently of the technique used for its production, might be indicative of the full potential of the planar model and highlights the limitations of a simplified laminated design and the need to move beyond it by including more complex features, such as mineral interlocking, to achieve full reproduction of the mechanical properties of natural nacre.

The improved tensile strength of the interlocked mineral composite also showed improved bending strength over the planar counterpart (Figure S9a). This enhanced bending strength has been reported in natural systems of similar characteristics and is a result of an interface that is strategically

https://dx.doi.org/10.1021/acsnano.0c01511
ACS Nano XXXX, XXX, XXX−XXX

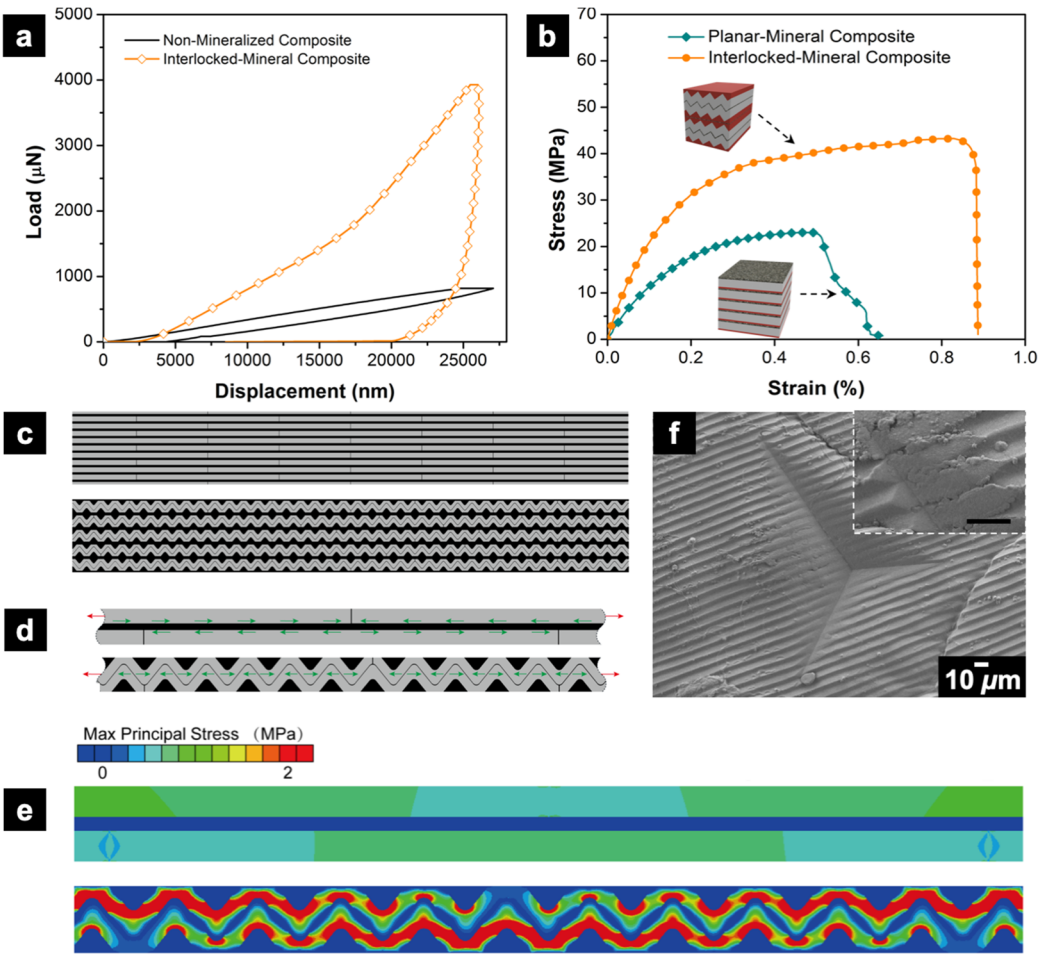

Figure 4. Mechanical property of the interlocked mineral composite. (a) Indentation on the mineralized (interlocked mineral) composites shows a higher stiffness (~25.8 GPa) than that of the nonmineralized composite. (b) Stress *vs* strain graph of the composites showing a higher tensile strength (~85%) and tensile toughness (~4 times higher) for the interlocked mineral composite than that of the planar counterpart. (c) Finite element method (FEM) models of the planar mineral composite and interlocked mineral composites. Comparison of (d) load transfer and (e) maximum principal stress field of planar mineral *vs* interlocked mineral composites under the same tensile load. In the planar mineral composite, load is transferred through the soft matrix, but in the interlocked mineral composite, load gets transferred directly through the stiffer mineral phase because of the interlocking. (f) Absence of cracks around the indentation site on the interlocked mineral composite.

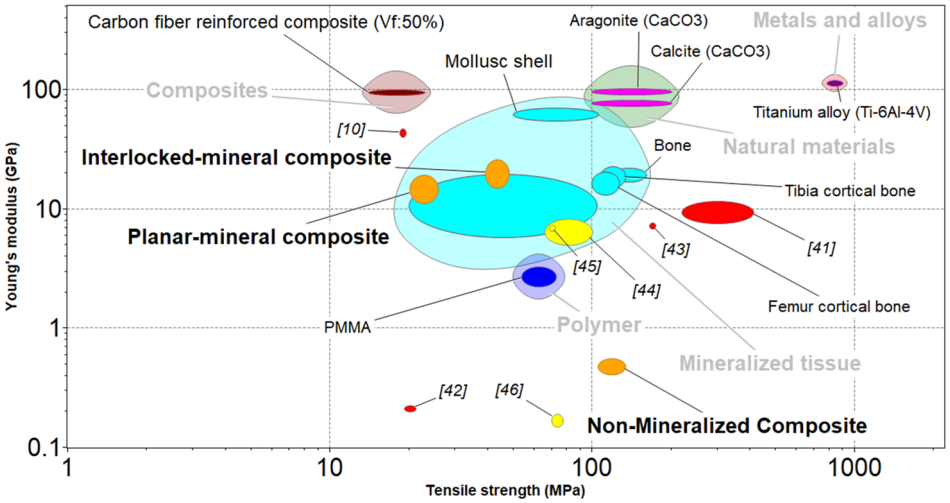

Figure 5. Comparison of mechanical properties. Elastic modulus *vs* ultimate tensile strength of the composite specimens juxtaposed against mineralized biological materials (bone and mollusc shell), common implantable materials (*e.g.*, Ti alloys), fiber-reinforced composites, and biomimetic $CaCO_3$-based (marked in red) and other Ca-based (marked in yellow) nacreous composites.[10,43−48]

https://dx.doi.org/10.1021/acsnano.0c01511
ACS Nano XXXX, XXX, XXX−XXX

designed to guide the propagation and dissipation of cracks.[22] In particular, the angled interfaces (with an interfacial angle between 30° and 40°) that were chosen here as a biological model have been reported to be effective in deflecting fissures.[20] This effect is clearly observed in the optical examination of the fractured regions of crossed-lamellar specimens, where the topography of the layers results in extended and tortuous deflections of the cracks, resulting in dissipation of fracture energy in the composite before causing complete fracture (Figure S9b). This effect can also be observed in the absence of surface cracks in the composite (Figure 4g) during indentation, which is a characteristic of monolithic aragonite but is absent in the biological organic–inorganic composites comprising the same mineral.[10] The flexural work-of-fracture (determined by integrating the area under the flexural stress–strain curve[39,40]) showed that the interlocked mineral composite have a 36% higher value than that of the plan mineral composites (Table ST1).

The approach of linking natural molecules with a design they evolve to follow is a complex task when compared to the reproduction of a biological design with materials of known manufacture. However, this additional complexity enables the exploration of enhanced synergies between components as well as seamless integration with biological systems, from the human body to entire ecosystems. This biocompatibility was demonstrated for the composite through the culturing and growth of a mammalian embryonic stem cell population for a week on the surface of the interlocked mineral composite reported here. The use of components of known biocompatibility resulted in a composite that supports the growth of these cells without any sign of cytotoxicity, suggesting the suitability of the composite for medical uses (Figure S10a,b). Interestingly, the structured minerals showed significant enhancement of cell proliferation compared to that of flat mineral platelets (Figure S10c), which was attributed to the additional anchor points on the surface of the former. Additionally, the structured platelets showed an ability to drive cell growth along the direction of the pattern, an effect previously reported for other structured surfaces of similar dimensions.[41,42]

CONCLUSION

In conclusion, we have demonstrated the reproduction of a nacre mimic using native components (namely, chitin and fibroin as the organic phase and calcium carbonate as the inorganic phase) by following a crossed-lamellar model. This result not only achieved the characteristic toughness of the planar lamellar model but also realized the multifunctionality of the native material by nearly duplicating the tensile strength of the composite without altering its low density and biocompatibility (Figure 5). This result was achieved by reorganizing the components rather than the composition, which demonstrated the interlocking phenomenon between the different mineral phases as a generalizable strategy for the development of multifunctional composites.

METHODS

Materials. Flexible PMMA sheets of 0.14 mm thickness were obtained from Goodfellow Cambridge Limited, UK. Chitosan (medium molecular weight, high degree of deacetylation; Sigma-Aldrich), degummed silk from *Bombyx mori* (Mielke's Fiber Arts USA), analytical grade $(NH_4)_2CO_3$, poly(acrylic acid) (M_w = 1800 g/mol), $CaCl_2{\cdot}2H_2O$, NaOH, and methanol were used as received. Polydimethylsiloxane (PDMS) templates with sawtooth topographical patterns were prepared using a SYLGARD 184 silicon elastomer kit. A Thorlab Inc. ruled reflective diffraction grating, 450/mm, 25.0 × 50.0 × 9.5 mm (GR2550-45031) was used as the master mold for replication of patterns into PDMS. Ultrapure Millipore water was used in all the experiments.

Fabrication of Patterned Chitosan Surface. Chitosan (medium molecular weight, high degree of deacetylation; Sigma-Aldrich) was dissolved at 2% and 3% w/v in 1% v/v acetic acid. A few drops of the chitosan solution were dispensed on PMMA sheets and pressed with a PDMS mold comprising the topographical pattern. The soft-imprinting was carried out until the chitosan film was dried, after which the PDMS mold was peeled off. Subsequently, the patterned chitosan film was submerged in NaOH 4% (w/v) for 10 min to neutralize the protonated amino groups and avoid further dissolution.[36] Finally, the films were extensively washed in deionized water to remove the remaining NaOH and dried at 37 °C.

Biomineralization of the Patterned Chitosan Films. Patterned aragonite was grown on the patterned chitosan substrates by using a PAA-based mineralization precursor comprising a 5 mM $CaCl_2$ solution and 10 μg/mL PAA and by implementing the traditional ammonia diffusion technique. The patterned chitosan films were submerged in the mineralization precursor held in a Petri dish, and the latter was covered with an Al foil with one perforation and then was placed inside a closed desiccator along with ∼2 g of NH_4HCO_3. The mineralization was performed for different durations (12, 18, 24 h) to determine the uniformity of mineral growth on the chitosan substrate.

Synthesis of Silk Fibroin. A 5% w/v silk fibroin aquous solution was prepared from degummed silk from *Bombyx mori* (Mielke's Fiber Arts USA) by implementing the protocol described in ref 36.

Structural and Chemical Characterization. The morphology of the aragonite laminates and the composite specimen were investigated using a JEOL JSM-7600F field-emission scanning electron microscope (FE-SEM) operating at an accelerating voltage of 5 kV. The XRD measurements of the mineralized $CaCO_3$ crystals were carried out with a Bruker D8 Discover high-resolution XRD with a Cu Kα1 source. The FTIR measurements for the chitosan (C) films, chitosan–silk films (CS), chitosan–aragonite (CA) laminates, and finally, the chitosan–aragonite laminates coated with silk (CAS) were performed with a resolution of 2 cm^{-1} between 4000 and 500 cm^{-1} (Vertex 70, Bruker, Germany) and analyzed with Essential FTIR (Operant LLC, USA).

Mechanical Characterization. An Instron 5940 single-column universal testing machine equipped with a 500 N load cell was used for the tensile testing of the composite specimens. Dog-bone-shaped specimens with a size of the reduced section of ∼1 mm width and 0.5 mm thickness were used. A minimum of 10 samples of each composite type were tested. The tensile toughness is obtained from the area under the tensile stress–strain curve between zero and ultimate strain.[36]

Three-point bending tests were also performed on the Instron 5940 universal testing machine. Beam-shaped composite specimens (of each type) of length 15 mm, width 2 mm, and thickness 2 mm were prepared. The bending test was conducted at a loading rate of 0.05 mm/min. A minimum of five samples of each composite type were tested. The flexural work-of-fracture is obtained by integrating the area under the flexural stress–strain curve.[39,40] The observation of crack propagation was performed on a composite beam-shaped specimen of the same dimensions, with a notch of 300 μm in the middle.

Indentation was performed using NanoTest NTX (Micro Materials Ltd., UK) equipped with a Berkovich indenter. For increased precision, indentation was repeated five times at 10 different sites (total of 50 indents per sample). The final depth of each indent never exceeded 10 percent of the sample thickness and was at least 4 times larger than the thickness of individual mineral layer present in the composite. A loading rate of 80 mN/s was used so that the loading and unloading time segments fell between 20 and 50 s. The reduced

https://dx.doi.org/10.1021/acsnano.0c01511
ACS Nano XXXX, XXX, XXX–XXX

modulus was calculated (by the Oliver–Pharr method),[49] and an average value was determined from all the tests for each sample.

Finite Element Analysis. Numerical simulations were conducted using the commercial FE package ABAQUS/Standard to capture the mechanical response of the tensile specimens. The stiff and soft materials were both generated by plane strain elements CEP4. For the stiff material, a linear elastic model is used with a Young's modulus of 100 GPa and a Poisson ratio of 0.3. For the soft material, the Young's modulus is 400 MPa and the Poisson ratio is 0.4. Geometric nonlinearities are considered to enable large deformation. In addition, finite element models used in the structure are verified by a mesh sensitivity test. To be consistent with the loading condition of the experiment in the simulation, the displacement of all nodes on the left side are constrained and lateral displacement is applied to the nodes on the right side of the specimen.

Embryonic Stem Cell Culture. Mouse embryonic stem cells (E14TG2A) purchased from ATCC, USA, were used for the biocompatibility study. These cells were cultured on a 0.1% (v/v) gelatin (Sigma-Aldrich,USA)-treated plate and supplemented with growth media, which consisted of DMEM (Nacalai Tesque, Japan),15% (v/v) FBS (Gibco, USA), 1% (v/v) sodium pyruvate (Thermo Fisher Scientific, USA), 0.1 mM (v/v) 2-β-mercaptoethanol (Thermo Fisher Scientific, USA) 1% L-Glutamax (Thermo Fisher Scientific, USA), 1% (v/v) pencillin–streptomycin, and 1000 U/mL leukemia inhibiting factor. The cell culture was performed at 37 °C and 5% CO_2. Media was reconstituted every other day. Upon 80% confluency the cells were detached from the Petri dish (Sigma-Aldrich, USA) by treating with a 0.25% of trypsin-EDTA solution (Nacalai Tesque, Japan) and 1×10^5 cells were taken for the biocompatibility experiment.

3D Cell Culturing and Characterization. The viability assay was carried out by using mouse embryonic stem cells (E14TG2A). These cells upon 80% confluence were trypsin treated to dissociate the cells from the Petri dish prior to seeding them on the sterilized composite specimen. The cells were then centrifuged and resuspended in the supplemented media before counting the cell number with a cell counter. The calcium carbonate biocomposite was sterilized with 70% ethanol for 15 min followed by UV exposure for another 15 min before inoculating the stem cells. A total of 1×10^5 cells were added onto both the patterned and nonpatterned composites. The samples were then incubated in the presence of growth medium at 37 °C, 5% CO_2. The samples were supplied with fresh media every 24 h. A LIVE/DEAD viability/cytotoxicity assay kit (Invitrogen, Thermo Fisher Scientific) was used to check the viability of the cells on the composite. The LIVE/DEAD stain was added to the samples and incubated for 30 min in the dark at 37 °C. The fluorescent images indicated for live cells (green) and for dead cells (red) were collected using an inverted microscope (Axio Observer, Carl Zeiss GmbH, Germany).

For SEM imaging of stem cells seeded on the composites, the cell-seeded composites were fixed with 4% paraformaldehyde for 10 min, followed by washing with 1× PBS for 10 min. The composites with cells were then put through a series of dehydration steps by treating with different percentages of ethanol concentrations. The gradient dehydration step was 50% ethanol for 5 min, 70% ethanol for 10 min, 80% ethanol for 10 min, 90% ethanol 5 min, three times each, and finally 100% ethanol for 5 min, three times each. The dehydrated cell seeded biocomposite was morphologically analyzed using SEM (JEOL JSM-7600F).

ASSOCIATED CONTENT

Supporting Information

The Supporting Information is available free of charge at https://pubs.acs.org/doi/10.1021/acsnano.0c01511.

Schematic of biomineralization process and XRD of the mineral, factors affecting biomineralization uniformity and exfoliation of the uniformly mineralized films, FT-IR spectra of the composite manufactured by bonding the mineralized films, additional cross-section images of the composite and determination of its mineral fraction, photograph of the nonmineralized composite showing shrinkage, flexural characterization of the mineralized composite and fracture propagation, cell viability studies on the composite demonstrating its biocompatibility, and table summarizing the mechanical characterization of the composite (PDF)

AUTHOR INFORMATION

Corresponding Authors

Caroline A. Ross − *Department of Materials Science and Engineering, Massachusetts Institute of Technology, Cambridge, Massachusetts 02139, United States;* orcid.org/0000-0003-2262-1249; Email: caross@mit.edu

Javier G. Fernandez − *Division of Engineering Product Development, Singapore University of Technology and Design, Singapore 487372, Republic of Singapore;* orcid.org/0000-0003-2961-6506; Email: javier.fernandez@sutd.edu.sg

Authors

Hemant Kumar Raut − *Department of Materials Science and Engineering, Massachusetts Institute of Technology, Cambridge, Massachusetts 02139, United States; Division of Engineering Product Development, Singapore University of Technology and Design, Singapore 487372, Republic of Singapore*

Alan F. Schwartzman − *Department of Materials Science and Engineering, Massachusetts Institute of Technology, Cambridge, Massachusetts 02139, United States*

Rupambika Das − *Division of Engineering Product Development, Singapore University of Technology and Design, Singapore 487372, Republic of Singapore*

Fan Liu − *Department of Mechanical Engineering, Stony Brook University, Stony Brook, New York 11794, United States*

Lifeng Wang − *Department of Mechanical Engineering, Stony Brook University, Stony Brook, New York 11794, United States;* orcid.org/0000-0002-2068-5102

Complete contact information is available at: https://pubs.acs.org/10.1021/acsnano.0c01511

Author Contributions

H.K.R., J.G.F., and C.R. conceived the idea. H.K.R. performed the fabrication and mechanical experiments. A.S. performed the mechanical tests. R.D. performed the biological experiments. F.L. and L.W. performed the finite element analysis. J.G.F. and C.R. supervised the work. J.G.F., H.K.R., and C.R. wrote the manuscript, with input of all the other authors.

Notes

The authors declare no competing financial interest.

ACKNOWLEDGMENTS

H.K.R. acknowledges funding from SUTD-MIT Postdoctoral Fellowship from Singapore University of Technology and Design. Shared facilities of CMSE, an NSF MRSEC under award DMR1419807, were used. This work was partially supported by the National Research Foundation, Singapore (grant number: CRP20-2017-0004). J.G.F. and H.K.R. thank SUTD-MIT International Design Centre (IDC) for the use of its shared facilities.

https://dx.doi.org/10.1021/acsnano.0c01511
ACS Nano XXXX, XXX, XXX−XXX

REFERENCES

(1) Fernandez, J. G.; Ingber, D. E. Bioinspired Chitinous Material Solutions for Environmental Sustainability and Medicine. *Adv. Funct. Mater.* **2013**, *23*, 4454−4466.

(2) Sanandiya, N. D.; Vijay, Y.; Dimopoulou, M.; Dritsas, S.; Fernandez, J. G. Large-Scale Additive Manufacturing with Bioinspired Cellulosic Materials. *Sci. Rep.* **2018**, *8*, 8642.

(3) Ritchie, R. O. The Conflicts between Strength and Toughness. *Nat. Mater.* **2011**, *10*, 817−822.

(4) Naleway, S. E.; Porter, M. M.; McKittrick, J.; Meyers, M. A. Structural Design Elements in Biological Materials: Application to Bioinspiration. *Adv. Mater.* **2015**, *27*, 5455−5476.

(5) Barthelat, F.; Yin, Z.; Buehler, M. J. Structure and Mechanics of Interfaces in Biological Materials. *Nat. Rev. Mater.* **2016**, *1*, 16007.

(6) Wang, J.; Cheng, Q.; Tang, Z. Layered Nanocomposites Inspired by the Structure and Mechanical Properties of Nacre. *Chem. Soc. Rev.* **2012**, *41*, 1111−1129.

(7) Wegst, U. G. K.; Bai, H.; Saiz, E.; Tomsia, A. P.; Ritchie, R. O. Bioinspired Structural Materials. *Nat. Mater.* **2015**, *14*, 23.

(8) Podsiadlo, P.; Kaushik, A. K.; Arruda, E. M.; Waas, A. M.; Shim, B. S.; Xu, J.; Nandivada, H.; Pumplin, B. G.; Lahann, J.; Ramamoorthy, A.; Kotov, N. A. Ultrastrong and Stiff Layered Polymer Nanocomposites. *Science* **2007**, *318*, 80.

(9) Munch, E.; Launey, M. E.; Alsem, D. H.; Saiz, E.; Tomsia, A. P.; Ritchie, R. O. Tough, Bio-Inspired Hybrid Materials. *Science* **2008**, *322*, 1516−1520.

(10) Mao, L.-B.; Gao, H.-L.; Yao, H.-B.; Liu, L.; Cölfen, H.; Liu, G.; Chen, S.-M.; Li, S.-K.; Yan, Y.-X.; Liu, Y.-Y.; Yu, S.-H. Synthetic Nacre by Predesigned Matrix-Directed Mineralization. *Science* **2016**, *354*, 107−110.

(11) Zhang, C.; McAdams Ii, D. A.; Grunlan, J. C. Nano/Micro-Manufacturing of Bioinspired Materials: A Review of Methods to Mimic Natural Structures. *Adv. Mater.* **2016**, *28*, 6292−6321.

(12) Le Ferrand, H.; Bouville, F.; Niebel, T. P.; Studart, A. R. Magnetically Assisted Slip Casting of Bioinspired Heterogeneous Composites. *Nat. Mater.* **2015**, *14*, 1172.

(13) Finnemore, A.; Cunha, P.; Shean, T.; Vignolini, S.; Guldin, S.; Oyen, M.; Steiner, U. Biomimetic Layer-By-Layer Assembly of Artificial Nacre. *Nat. Commun.* **2012**, *3*, 966.

(14) Zhang, Y.; Heim, F. M.; Bartlett, J. L.; Song, N.; Isheim, D.; Li, X. Bioinspired, Graphene-Enabled Ni Composites with High Strength and Toughness. *Sci. Adv.* **2019**, *5*, No. eaav5577.

(15) Liu, P.; Jin, Z.; Katsukis, G.; Drahushuk, L. W.; Shimizu, S.; Shih, C.-J.; Wetzel, E. D.; Taggart-Scarff, J. K.; Qing, B.; Van Vliet, K. J.; Li, R.; Wardle, B. L.; Strano, M. S. Layered and Scrolled Nanocomposites with Aligned Semi-Infinite Graphene Inclusions at the Platelet Limit. *Science* **2016**, *353*, 364.

(16) Bouville, F.; Maire, E.; Meille, S.; Van de Moortèle, B.; Stevenson, A. J.; Deville, S. Strong, Tough and Stiff Bioinspired Ceramics from Brittle Constituents. *Nat. Mater.* **2014**, *13*, 508−514.

(17) Zhao, H.; Yue, Y.; Guo, L.; Wu, J.; Zhang, Y.; Li, X.; Mao, S.; Han, X. Cloning Nacre's 3D Interlocking Skeleton in Engineering Composites to Achieve Exceptional Mechanical Properties. *Adv. Mater.* **2016**, *28*, 5099−5105.

(18) Grossman, M.; Bouville, F.; Erni, F.; Masania, K.; Libanori, R.; Studart, A. R. Mineral Nano-Interconnectivity Stiffens and Toughens Nacre-Like Composite Materials. *Adv. Mater.* **2017**, *29*, 1605039.

(19) Zhang, Y.; Li, X. Bioinspired, Graphene/Al2o3 Doubly Reinforced Aluminum Composites with High Strength and Toughness. *Nano Lett.* **2017**, *17*, 6907−6915.

(20) Mirkhalaf, M.; Dastjerdi, A. K.; Barthelat, F. Overcoming the Brittleness of Glass through Bio-Inspiration and Micro-Architecture. *Nat. Commun.* **2014**, *5*, 3166.

(21) Mirkhalaf, M.; Zhou, T.; Barthelat, F. Simultaneous Improvements of Strength and Toughness in Topologically Interlocked Ceramics. *Proc. Natl. Acad. Sci. U. S. A.* **2018**, *115*, 9128.

(22) Gu, G. X.; Takaffoli, M.; Buehler, M. J. Hierarchically Enhanced Impact Resistance of Bioinspired Composites. *Adv. Mater.* **2017**, *29*, 1700060.

(23) Li, X.; Chang, W.-C.; Chao, Y. J.; Wang, R.; Chang, M. Nanoscale Structural and Mechanical Characterization of a Natural Nanocomposite Material: The Shell of Red Abalone. *Nano Lett.* **2004**, *4*, 613−617.

(24) Li, X.; Xu, Z.-H.; Wang, R. *In Situ* Observation of Nanograin Rotation and Deformation in Nacre. *Nano Lett.* **2006**, *6*, 2301−2304.

(25) Li, X. W.; Ji, H. M.; Yang, W.; Zhang, G. P.; Chen, D. L. Mechanical Properties of Crossed-Lamellar Structures in Biological Shells: A Review. *J. Mech. Behav. Biomed. Mater.* **2017**, *74*, 54−71.

(26) Almagro, I.; Drzymała, P.; Berent, K.; Sainz-Díaz, C. I.; Willinger, M. G.; Bonarski, J.; Checa, A. G. New Crystallographic Relationships in Biogenic Aragonite: The Crossed-Lamellar Microstructures of Mollusks. *Cryst. Growth Des.* **2016**, *16*, 2083−2093.

(27) Kamat, S.; Su, X.; Ballarini, R.; Heuer, A. H. Structural Basis for the Fracture Toughness of the Shell of the Conch *Strombus gigas*. *Nature* **2000**, *405*, 1036−1040.

(28) Shin, Y. A.; Yin, S.; Li, X.; Lee, S.; Moon, S.; Jeong, J.; Kwon, M.; Yoo, S. J.; Kim, Y.-M.; Zhang, T.; Gao, H.; Oh, S. H. Nanotwin-Governed Toughening Mechanism in Hierarchically Structured Biological Materials. *Nat. Commun.* **2016**, *7*, 10772.

(29) Li, L.; Ortiz, C. A Natural 3D Interconnected Laminated Composite with Enhanced Damage Resistance. *Adv. Funct. Mater.* **2015**, *25*, 3463−3471.

(30) Aitken, Z. H.; Luo, S.; Reynolds, S. N.; Thaulow, C.; Greer, J. R. Microstructure Provides Insights into Evolutionary Design and Resilience of *Coscinodiscus Sp.* Frustule. *Proc. Natl. Acad. Sci. U. S. A.* **2016**, *113*, 2017.

(31) Li, X.; Huang, Z. Unveiling the Formation Mechanism of Pseudo-Single-Crystal Aragonite Platelets in Nacre. *Phys. Rev. Lett.* **2009**, *102*, No. 075502.

(32) Kato, T. Polymer/Calcium Carbonate Layered Thin-Film Composites. *Adv. Mater.* **2000**, *12*, 1543−1546.

(33) Fernandez, J. G.; Mills, C. A.; Pla-Roca, M.; Samitier, J. Forced Soft Lithography (Fsl): Production of Micro- and Nanostructures in Thin Freestanding Sheets of Chitosan Biopolymer. *Adv. Mater.* **2007**, *19*, 3696−3701.

(34) Fernandez, J. G.; Mills, C. A.; Martinez, E.; Lopez-Bosque, M. J.; Sisquella, X.; Errachid, A.; Samitier, J. Micro- and Nanostructuring of Freestanding, Biodegradable, Thin Sheets of Chitosan *via* Soft Lithography. *J. Biomed. Mater. Res., Part A* **2008**, *85A*, 242−247.

(35) Nielsen, M. H.; Aloni, S.; De Yoreo, J. J. *In Situ* Tem Imaging of Caco3 Nucleation Reveals Coexistence of Direct and Indirect Pathways. *Science* **2014**, *345*, 1158.

(36) Fernandez, J. G.; Ingber, D. E. Unexpected Strength and Toughness in Chitosan-Fibroin Laminates Inspired by Insect Cuticle. *Adv. Mater.* **2012**, *24*, 480−484.

(37) Fernandez, J. G.; Mills, C. A.; Samitier, J. Complex Microstructured 3D Surfaces Using Chitosan Biopolymer. *Small* **2009**, *5*, 614−620.

(38) Grossman, M.; Bouville, F.; Masania, K.; Studart, A. R. Quantifying the Role of Mineral Bridges on the Fracture Resistance of Nacre-Like Composites. *Proc. Natl. Acad. Sci. U. S. A.* **2018**, *115*, 12698.

(39) Bai, H.; Walsh, F.; Gludovatz, B.; Delattre, B.; Huang, C.; Chen, Y.; Tomsia, A. P.; Ritchie, R. O. Bioinspired Hydroxyapatite/Poly(Methyl Methacrylate) Composite with a Nacre-Mimetic Architecture by a Bidirectional Freezing Method. *Adv. Mater.* **2016**, *28*, 50−56.

(40) Eckert, A.; Rudolph, T.; Guo, J.; Mang, T.; Walther, A. Exceptionally Ductile and Tough Biomimetic Artificial Nacre with Gas Barrier Function. *Adv. Mater.* **2018**, *30*, 1802477.

(41) Puckett, S.; Pareta, R.; Webster, T. J. Nano Rough Micron Patterned Titanium for Directing Osteoblast Morphology and Adhesion. *Int. J. Nanomed.* **2008**, *3*, 229−241.

(42) Mills, C. A.; Fernandez, J. G.; Martinez, E.; Funes, M.; Engel, E.; Errachid, A.; Planell, J.; Samitier, J. Directional Alignment of Mg63 Cells on Polymer Surfaces Containing Point Microstructures. *Small* **2007**, *3*, 871−879.

https://dx.doi.org/10.1021/acsnano.0c01511
ACS Nano XXXX, XXX, XXX−XXX

(43) Bonderer, L. J.; Studart, A. R.; Gauckler, L. J. Bioinspired Design and Assembly of Platelet Reinforced Polymer Films. *Science* **2008**, *319*, 1069.
(44) Abdolmohammadi, S.; Siyamak, S.; Ibrahim, N. A.; Yunus, W. M.; Rahman, M. Z.; Azizi, S.; Fatehi, A. Enhancement of Mechanical and Thermal Properties of Polycaprolactone/Chitosan Blend by Calcium Carbonate Nanoparticles. *Int. J. Mol. Sci.* **2012**, *13*, 4508−22.
(45) Saito, T.; Oaki, Y.; Nishimura, T.; Isogai, A.; Kato, T. Bioinspired Stiff and Flexible Composites of Nanocellulose-Reinforced Amorphous Caco3. *Mater. Horiz.* **2014**, *1*, 321−325.
(46) Sousa, R. A.; Reis, R. L.; Cunha, A. M.; Bevis, M. J. Processing and Properties of Bone-Analogue Biodegradable and Bioinert Polymeric Composites. *Compos. Sci. Technol.* **2003**, *63*, 389−402.
(47) Abu Bakar, M. S.; Cheang, P.; Khor, K. A. Mechanical Properties of Injection Molded Hydroxyapatite-Polyetheretherketone Biocomposites. *Compos. Sci. Technol.* **2003**, *63*, 421−425.
(48) Guo, Y.-P.; Guan, J.-J.; Yang, J.; Wang, Y.; Zhang, C.-Q.; Ke, Q.-F. Hybrid Nanostructured Hydroxyapatite−Chitosan Composite Scaffold: Bioinspired Fabrication, Mechanical Properties and Biological Properties. *J. Mater. Chem. B* **2015**, *3*, 4679−4689.
(49) Oliver, W. C.; Pharr, G. M. An Improved Technique for Determining Hardness and Elastic Modulus Using Load and Displacement Sensing Indentation Experiments. *J. Mater. Res.* **1992**, *7*, 1564−1583.

https://dx.doi.org/10.1021/acsnano.0c01511
ACS Nano XXXX, XXX, XXX−XXX